Carbonate-Assisted Hydrothermal Synthesis of Nanoporous CuO Microstructures and Their Application in Catalysis

Min Zhou,*[a] Yan'an Gao,[b] Baoxiang Wang,[a] Zbigniew Rozynek,[a] and Jon Otto Fossum[a]

We have demonstrated a facile carbonate-assisted hydrothermal route for synthesis of well-defined nanoporous copper oxide microstructures with high surface area. The nanoporous CuO microstructures were synthesised by adding sodium hydrogen carbonate ($NaHCO_3$) to an aqueous solution of copper chloride ($CuCl_2$) in the presence of poly(vinylpyrrolidone) (PVP) at 300 °C. The introduction of $NaHCO_3$ is critical for the successful synthesis of porous nanoarchitectures owing to the formation of carbon dioxide (CO_2) gas during the synthesis process. The structure and morphology of CuO are very sensitive to the concentration of $NaHCO_3$ and PVP, as well as to the molecular weight of PVP. The nanoporous CuO product shows higher catalytic activity than other types of CuO materials because of its porous structure. It is believed that this method will provide a simple and versatile approach to large-scale production of CuO with high surface area by means of a facile hydrothermal route.

Introduction

Porous materials have attracted great interest because of their wide application in the fields of catalysis,[1–3] sensors,[4–6] environmental engineering[7,8] and drug delivery[9–11] owing to their high surface-to-volume ratio and ability to interact with ions, atoms and molecules, not only at the surface but also throughout the bulk of the materials. Thus, changing the structure of these materials from solid to porous provides a potential way to improve their properties and application.

As an important functional metal oxide, CuO, a p-type semiconductor with narrow band gap (E_g = 1.2 eV),[12] has attracted great attention because of its unique properties and widespread potential applications in optical switches, field emitters, gas sensors and high-temperature microconductors.[13–19] Recently, CuO has been revisited as an efficient material for the preparation of Li-ion battery anode materials[14] and can be used as a promising catalyst for the complete conversion of hydrocarbons into carbon dioxide and water.[20–23] In addition, it has been applied as a photoelectrode for water splitting aimed at hydrogen production, in order to convert solar energy into storable chemical energy.[24] With the decrease in crystal size, CuO nanostructures may exhibit unique properties that could be signifi-

cantly different from those of their bulk. Therefore, it is reasonable to believe that the ability to process bulk CuO into nanostructured materials should enrich our understanding of its fundamental properties and enhance its performance in currently existing applications. So far, CuO nanostructures with different shapes including nanoparticles, nanorods, nanowires, nanosheets, nanoflowers, etc. have been synthesised by a variety of techniques such as wet chemical,[14,25] hydrothermal or solvothermal,[26,27] electrochemical,[28] microwave-induced,[29] thermal oxidation,[13] reaction in micelles[30] and solid–liquid arc discharge methods.[15] For example, Zeng et al.[31] used a wet chemical method in water-ethanol mixed solvents at 77–82 °C and 1 atm to get one-dimensional CuO nanostructures such as nanorods and nanoribbons. Use of a two-tiered organising scheme with multiple-length scales for construction produced dandelion-like hollow CuO microspheres.[32] Xiao and co-workers[33] reported the preparation of CuO nanorods, nanobranches and nanoflasks by a hydrothermal route in the presence of sodium citrate. Liu et al.[18] prepared CuO with honeycomb and flower-like morphologies by an anion-controlled self-assembly route, and the presence of WO_4^{2-} and MnO_4^{2-} helped in the construction of CuO nanoarchitectures on copper foils. In addition, CuO materials with nanoribbon and nanoring morphologies were successfully fabricated by the simple solution-phase reaction of $CuCl_2$ and NaOH with sodium dodecylbenzenesulfonate.[19] To the best of our knowledge, however, most of these CuO nanomaterials are solid structures; there are few reports concerning the fabrication of CuO nanoarchitectures with porous structures. The highly porous CuO is of great interest because of its enhanced sur-

[a] Department of Physics, Norwegian University of Science and Technology (NTNU),
Høgskoleringen 5, 7491 Trondheim, Norway
Fax: +47-73597710
E-mail: min.zhou@ntnu.no
[b] Max Planck Institute for Dynamics of Complex Technical Systems,
Sandtorstrasse 1, 39106 Magdeburg, Germany

face-to-volume ratios for sensing and catalytic applications and for its potential use as a transparent conducting oxide with extremely large surface area for photovoltaic, electro-optic or battery devices.

Herein, we demonstrate that nanoporous CuO microstructures can be easily obtained by a facile carbonate-assisted hydrothermal approach in the presence of a nonionic water soluble polymer, PVP. In contrast to other hydrothermal approaches, this paper introduces $NaHCO_3$ to the system, which has a great effect on the formation of the nanoporous CuO microstructures under certain experimental conditions. A large quantity of CO_2 is formed during the high-temperature reaction process when $NaHCO_3$ is added to the reaction solution, and well-defined nanoporous CuO microstructures are produced because of the formation of CO_2. On the basis of our results, we believe that both the molecular weight and concentration of PVP significantly affect the morphologies of the final products. This facile approach has potential for large-scale synthesis of nanoporous materials, and it can also be extended to the synthesis of other metal oxide nanoporous structures with high surface areas.

Figure 1. (a) Representative panoramic SEM image of the CuO microstructures obtained by adding of $NaHCO_3$ (10 mL, 500 mM) into $CuCl_2$ (10 mL, 250 mM) solution in the presence of poly(vinylpyrrolidone) (K15, 0.05 g). (b) Low-magnification images of a similar area of CuO microstructures. (c,d) Individual quasi-spheres and octahedral structures. (e) High-magnification images of the quasi-spheres clearly indicate the nanoporous structure of the samples.

Results and Discussion

The nanoporous CuO microstructures were synthesised by using $CuCl_2$ as a copper precursor, $NaHCO_3$ as the agent for controlling the porosity and PVP as the regulator of morphology. Firstly, $NaHCO_3$ (10 mL, 500 mM) was added to the $CuCl_2$ solution (10 mL, 250 mM) in the presence of PVP (0.01 g). The mixture was shaken for 10 s and then transferred to an autoclave for the hydrothermal process. Figure 1 shows the SEM images of typical nanoporous CuO microstructures synthesised by the hydrothermal approach. Figure 1a shows the panoramic SEM image of this product. One can see that the sample consists of spherical particles that are usually 0.6–1.0 μm in diameter, with an average of about 0.8 μm. The SEM image in Figure 1b indicates that the particles are composed of a large number of irregular quasi-spheroid particles, clearly revealing that all these quasi-spheres have some corners. Some well-defined octahedral microstructures are also found with sizes of about 0.6 μm (see arrow in Figure 1b). Figures 1c and 1d show higher-magnification images of individual quasi-spheroids and octahedral particles. The magnified SEM images as shown in Figure 1e demonstrate that the irregular spheres have porous structures with a pore size of about 16 nm.

Nitrogen physisorption represents the most extensively used technique to measure catalyst surface area and to study the texture of pores. The porosity of the CuO microstructures is further revealed by the N_2 adsorption/desorption isothermal curve illustrated in Figure 2a. The Brunauer–Emmett–Teller (BET) surface area of the porous microstructure is 30.04 m²/g, and the pore size distribution curve in the inset exhibits bimodal pore distribution. The pores at about 18 and 190 nm originate from the surface
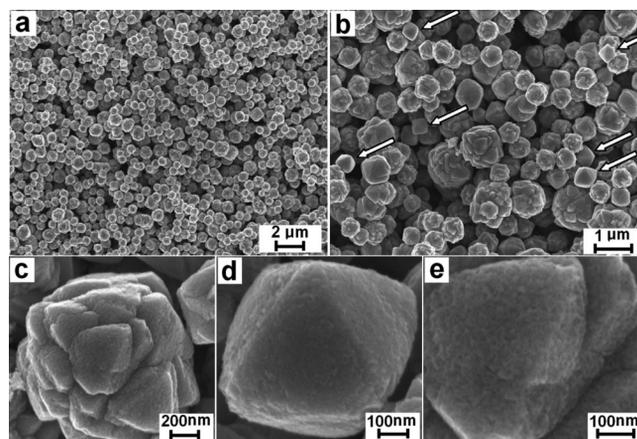
pore formed by the release of CO_2 and the gaps between two quasi-spheres, respectively, which can be confirmed directly by the SEM observation (Figure 1).
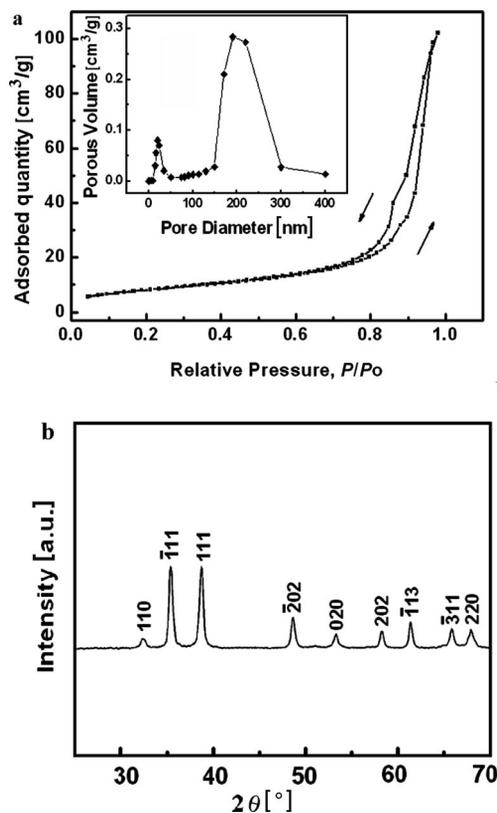

Figure 2. N_2 adsorption/desorption isothermal curve (a) and the XRD pattern (b) of the nanoporous CuO. The inset of (a) shows the corresponding pore size distribution.

EurJIC
European Journal
of Inorganic Chemistry

XRD patterns, as the one shown in Figure 2b, were employed to analyse the crystal structure of the samples obtained in aqueous solution. The diffraction peaks can, by comparison with the respective JCPDS card No. 05–0661, be indexed to be in good agreement with the monoclinic phase structure of CuO. The strong and sharp peaks indicate that the CuO product was high in purity and had a high degree of crystallinity. No other peaks were detected, which suggests that the presence of PVP has little influence on the phase of the final products. XRD analysis of the samples reveals the formation of the monoclinic phase structure of CuO having lattice parameters consistent with those reported in the literature.[3,15,20]

In our synthesis we found that, by controlling experimental parameters such as molecular weight and concentration of PVP, various structures and morphologies of CuO can be obtained. The different morphologies of the CuO microstructures shown in Figure 3 are varied by only changing the concentration of NaHCO$_3$. When the concentration of NaHCO$_3$ was decreased to 100 mM, microspheres with a hierarchical structure and an average size of about 11 µm were obtained (Figure 3a). The images of an individual sphere and its highly magnified surface are shown in Figure 3b,c. It can be seen that there are numerous nanostructures, which display rod-like profiles, on the surface of the
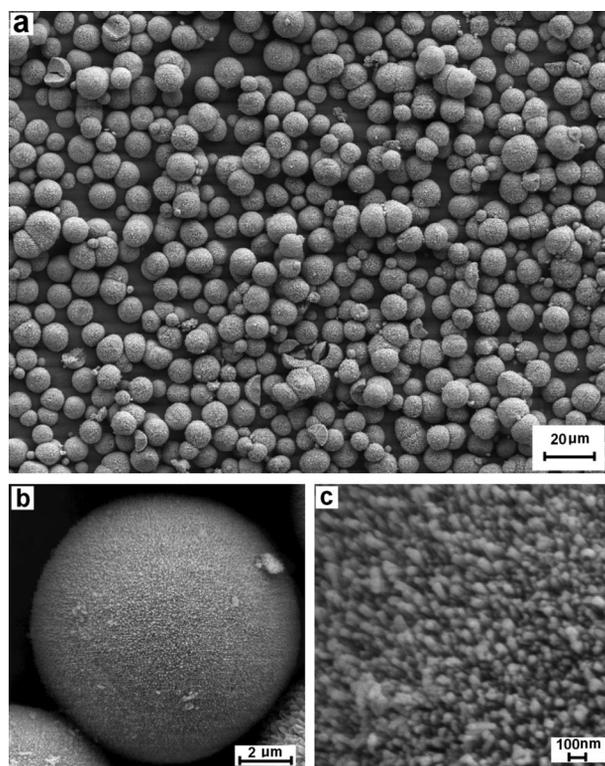
microsphere. The final morphology of these microspheres can be easily controlled; more than 90% of the morphologies yield CuO microspheres with hierarchical structures. We also found that product morphology is sensitive to the type of the PVP employed. Here we used three kinds of PVP with different molecular weights, PVPK90 (M_w = 360,000), PVPK30 (M_w = 40,000) and PVPK15 (M_w = 10,000). When the molecular weight of PVP was increased to 40,000 (PVPK30), lamellar microstructures with a size of 1.4 µm were obtained (Figure 4a). From the magnified SEM image (Figure 4b), it is clear that numerous microplates assemble to form the lamellar microstructures. Increasing the molecular weight further to 360,000 changes the shape of the products to flower-like microstructures (Figure 4c,d). These microflowers are composed of several microplates with a size and thickness of about 1 µm and 40 nm, respectively. It is also worthwhile mentioning that the concentration of PVP in the reaction solution is an important factor in determining the morphology of the final CuO products. By decreasing this concentration to 0.1 mg/mL of PVPK15, for example, urchin-like microstructures composed of rod-like building units are created. Lower- and higher-magnification images illustrate the urchin-like structures and indicate that the length and width of these small nanorods are about 800 nm and 60 nm, respectively (Figure 5a,b). When the polymer (PVPK15) concentration is increased to 20 mg/mL, the CuO products are hollow microspheres with a size of about 8 µm (Figure 5c). The magnified SEM image (Figure 5d) demonstrates clearly the hollow structures of the products. These results confirm that PVP plays an important role in the hydrothermal process.

Figure 3. SEM images of CuO products obtained without NaHCO$_3$ under otherwise identical conditions [CuCl$_2$ (10 mL, 250 mM) and PVPK15 (0.05 g)]: (a) Low-magnification image showing many microspheres; (b) higher-magnification image showing one microsphere; (c) high-magnification image showing the surface of a microsphere.
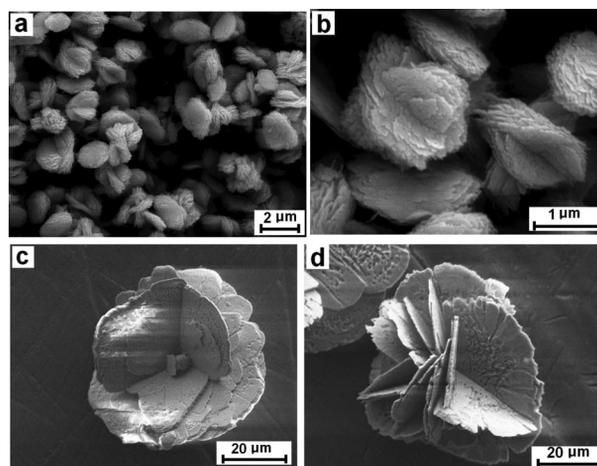

Figure 4. SEM images of the CuO samples produced with high- and low-molecular-weight PVP, K30 (a,b) and K90 (c,d), respectively.

During the formation of the porous microstructures, NaHCO$_3$ affects the structure and PVP affects the morphologies of the final products. The reactions involved in our system are shown below [Equation (1) and Equation (2)]:
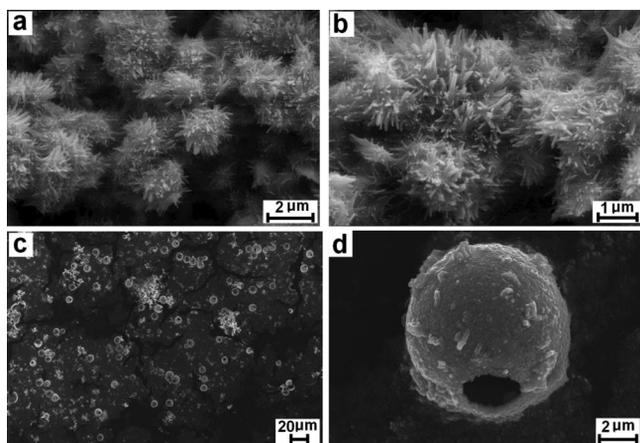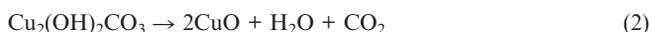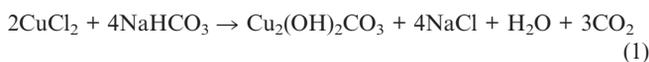
Figure 5. SEM images of the CuO samples produced with high (a,b) and low (c,d) concentrations of PVPK15.

$$2CuCl_2 + 4NaHCO_3 \rightarrow Cu_2(OH)_2CO_3 + 4NaCl + H_2O + 3CO_2 \quad (1)$$

$$Cu_2(OH)_2CO_3 \rightarrow 2CuO + H_2O + CO_2 \quad (2)$$

In this hydrothermal system, we believe that a two-step chemical reaction involving a synthesis and a decomposition occurs. In the synthesis step, when $NaHCO_3$ was added to the $CuCl_2$ solution, a blue coloured precipitate was observed immediately in the system, indicating the formation of $Cu_2(OH)_2CO_3$. Then, the reaction mixture was transferred to an autoclave. The decomposition step occurred at the decomposition temperature of $Cu_2(OH)_2CO_3$. Decomposition produced solid CuO, H_2O and CO_2 gas. Finally, a large number of nanoscale pores formed on the surface of the products due to the release of carbon dioxide gas from the copper carbonate. The control experiment illustrated in Figure 6 shows that no porous structures can be formed without addition of $NaHCO_3$. Therefore, the introduction of $NaHCO_3$ is a decisive factor in the formation of porous CuO.
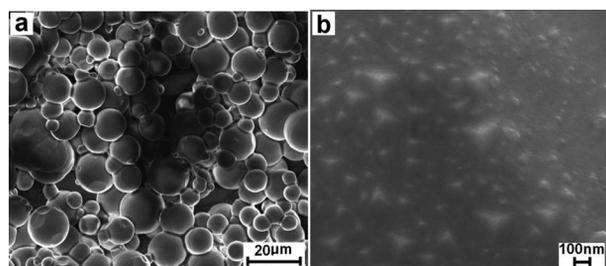

Figure 6. High- (a) and low-magnification (b) SEM images of the CuO microstructures obtained without $NaHCO_3$ under otherwise identical conditions [$CuCl_2$ (10 mL, 250 mM) and PVP K15 (0.05 g)].

Another important factor in the morphology of the final products is PVP. According to the experimental results, both the molecular weight and concentration of PVP, have a significant influence on the final morphology and structure of these CuO microstructures. PVP, as an important

capping agent, has been widely used in the synthesis of various nanostructures, including nanorods, nanowires, nanoplates and nanocubes. Although the exact function of PVP on the shape selectivity in our synthetic system is not yet fully understood, we believe that the selective adsorption of PVP on various crystallographic planes of newly formed CuO suppresses their intrinsic anisotropic growth. PVP containing an N–C=O group is easily attached to the surface of these CuO materials and slows down the growth of the crystal faces. As a kinetic controller of the growth rates of different crystalline faces through adsorption and desorption, PVP adsorption on specific crystalline surfaces could significantly decrease their growth rates and lead to a highly anisotropic growth. Selective interactions between PVP and the different surface planes of the CuO may greatly influence the growth direction and rate and ultimately result in particles with different shapes.

The catalytic activity of the nanoporous CuO samples in the oxidation of CO was evaluated. The resulting nanoporous CuO microstructures gave 100% conversion of CO at 160 °C, which is clearly lower than the corresponding temperatures for other nonporous CuO samples, such as microspheres and microflowers, which afford 100% conversion at 200 and 220 °C, respectively. No catalyst deactivation was observed during several activity test cycles. To elucidate the remarkable effects of the structure and morphology of the catalyst, the specific reaction rates were calculated and are given in Figure 7. At 160 °C, the specific reaction rates were 1.0, 1.5 and 7.3×10^{-8} $mol_{CO}/mol_{cat}/s$ for the microflowers, microspheres and porous microstructures, respectively; the rate on the porous microstructures is over seven times higher than that on the microflowers and over four times higher than that on microspheres.
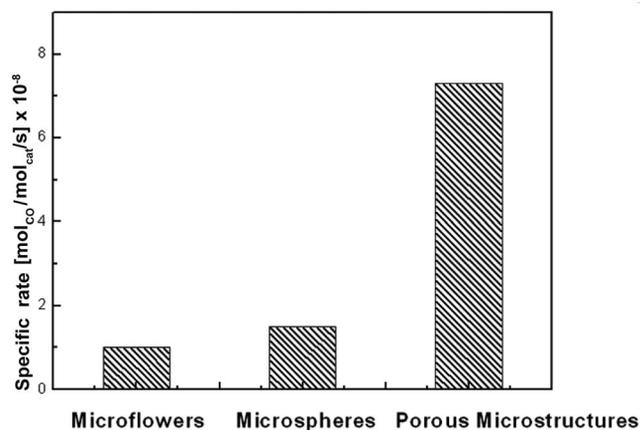

Figure 7. Specific rates of CO conversion as compared to CuO microflowers, microspheres and porous microstructures at 110 °C.

Catalytic oxidation of CO is not only an important reaction for many applications, such as removal of exhaust gas and in fuel cells, but it is also a fundamental process involving surface oxygen and oxygen vacancy participation. CuO materials have been of considerable interest, as they have been found to be effective catalysts for CO. Previous studies

suggest that such a reaction is a surface-area-sensitive process. It is well known that the activation barrier of the catalysed CO oxidation reaction over transition-metal surfaces is determined by the breaking of the metal–oxygen bond. Therefore, the surface properties of the CuO catalysts are strongly related to the nature of the surface used in the experiments. The ease of oxygen abstraction from the surface of CuO depends on the surface area and determines the catalytic activity. The effectiveness of an oxidation catalyst is mainly attributed to the adsorption and desorption of gas molecules from its surface. The higher surface area can enable a large fraction of the atoms to be present at the surface, which permits more gas molecules to enter and approach the active position easily. Thus, the catalytic activity of the nanoporous CuO microstructures described here can be caused by the large surface area and the pores with uniform sizes, which favour greater exposure of the surfaces to the gas molecules more effectively.

Conclusions

We present a facile and effective method for the synthesis of nanoporous CuO microstructures. The nanoporous CuO microstructures can be synthesised by controlling a few critical experimental parameters. It was found that the introduction of $NaHCO_3$ in the process plays an important role in the formation of the porous structure of the CuO products and that the molecular weight and concentration of PVP is a critical factor in controlling the morphology of the products. The nanoporous CuO microstructures exhibit good catalytic activity in the oxidation of CO, as compared with the CuO microsphere and CuO microflower products. The present results indicate that the synthesis of porous structures may by helpful for designing novel catalysts with desired performance. The successful preparation of these abundant and nanoporous CuO microstructures is relatively simple and very effective. This versatile route can also be extended to the synthesis of other metal oxide nanoporous structures with high surface area such as nickel, iron and so on.

Experimental Section

Hydrothermal Synthesis of Nanoporous CuO Microstructures: Copper(II) chloride ($CuCl_2 \cdot 2H_2O$, 99.0%) was purchased from Sigma–Aldrich, sodium hydrogen carbonate ($NaHCO_3$, 99–100%) was supplied by J. T. Baker. Three kinds of poly(vinylpyrrolidone) (PVPK90 M_w = 360,000, PVPK30 M_w = 40,000, and PVPK15 M_w = 10,000) were purchased from Fluka. All chemicals were used as received without further purification. Deionised water was used throughout. Copper oxide microstructures with various morphologies were synthesised in a solution process under ambient conditions. In a typical synthesis procedure, a given amount of PVP and $CuCl_2$ (0.25 mmol) were dissolved in deionised water (10 mL), and the mixture was dispersed to form a homogeneous solution by vigorous stirring at room temperature. Then, deionised water (10 mL) containing $NaHCO_3$ (500 mM) was quickly added to the above solution at room temperature. After 10 s of shaking, the mixture

solution was transferred to a 50 mL Teflon-lined autoclave. The autoclave was then sealed in a stainless steel tank and kept at 300 °C for 5 h. The reactor was then naturally cooled to room temperature. The resulting samples were collected and washed three times with deionised water. Then, the samples were dried in air at room temperature. Different structures and morphologies of products were obtained by varying synthetic parameters such as the concentration of $NaHCO_3$ or the concentration and molecular weight of PVP..

Characterisation: The general morphologies of the samples were characterised by a field-emission scanning electron microscope (FE-SEM, Leo 1530 Gemini). Powder X-ray diffraction (XRD) patterns were recorded by means of a diffractometer (Rigaku D/Max 2200) with Cu-K_α radiation (λ = 1.5406 Å). Brunauer–Emmett–Teller (BET) surface area measurements were performed with a Micromeritics ASAP-2000 nitrogen adsorption apparatus. The catalytic activities for CO oxidation were evaluated in a fixed-bed quartz tubular reactor. CuO particles (100 mg) were placed in the reactor. The reactant gases (1.0% CO, 16% O_2 balanced with N_2) went through the reactor at a flow rate of 100 mL/min and a gas hourly space velocity (GHSV) of about 12,000 h^{-1}. The products were analysed by a gas chromatograph equipped with a TDX column.

[1] S. H. Joo, S. J. Choi, I. Oh, J. Kwak, Z. Liu, O. Terasaki, R. Ryoo, *Nature* **2001**, *412*, 169–172.

[2] D. R. Rolison, *Science* **2003**, *299*, 1698–1702.

[3] J. Biener, A. Wittstock, L. A. Zepeda-Ruiz, M. M. Biener, V. Zielasek, D. Kramer, R. N. Viswanath, J. Weissmuller, M. Baumer, A. V. Hamza, *Nat. Mater.* **2009**, *8*, 47–51.

[4] Y. Y. Li, F. Cunin, J. R. Link, T. Gao, R. E. Betts, S. H. Reiver, V. Chin, S. N. Bhatia, M. J. Sailor, *Science* **2003**, *299*, 2045–2047.

[5] K. Bonroy, J. M. Friedt, F. Frederix, W. Laureyn, S. Langerock, A. Campitelli, M. Sara, G. Borghs, B. Goddeeris, P. Declerck, *Anal. Chem.* **2004**, *76*, 4299–4306.

[6] L. De Stefano, L. Rotiroti, I. Rendina, L. Moretti, V. Scognamiglio, M. Rossi, S. D′Auria, *Biosens. Bioelectron.* **2006**, *21*, 1664–1667.

[7] A. Bianchi, M. P. Papini, A. Corsi, P. Behra, M. Beccari, *Water Sci. Technol.* **2003**, *48*, 9–16.

[8] L. Chen, D. A. Sabatini, T. C. Kibbey, *Environ. Sci. Technol.* **2008**, *42*, 1916–1921.

[9] N. Tsapis, D. Bennett, B. Jackson, D. A. Weitz, D. A. Edwards, *Proc. Natl. Acad. Sci. USA* **2002**, *99*, 12001–12005.

[10] C. Y. Lai, B. G. Trewyn, D. M. Jeftinija, K. Jeftinija, S. Xu, S. Jeftinija, V. S. Lin, *J. Am. Chem. Soc.* **2003**, *125*, 4451–4459.

[11] E. J. Anglin, L. Cheng, W. R. Freeman, M. J. Sailor, *Adv. Drug Delivery Rev.* **2008**, *60*, 1266–1277.

[12] Y. L. Liu, L. Liao, J. C. Li, C. X. Pan, *J. Phys. Chem. C* **2007**, *111*, 5050–5056.

[13] X. C. Jiang, T. Herricks, Y. N. Xia, *Nano Lett.* **2002**, *2*, 1333–1338.

[14] X. P. Gao, J. L. Bao, G. L. Pan, H. Y. Zhu, P. X. Huang, F. Wu, D. Y. Song, *J. Phys. Chem. B* **2004**, *108*, 5547–5551.

[15] W. T. Yao, S. H. Yu, Y. Zhou, J. Jiang, Q. S. Wu, L. Zhang, J. Jiang, *J. Phys. Chem. B* **2005**, *109*, 14011–14016.

[16] M. Kaur, P. Muthe, S. K. Despande, S. Choudhury, J. B. Singh, N. Verma, S. K. Gupta, J. V. Yakhmi, *J. Cryst. Growth* **2006**, *289*, 670–675.

M. Zhou, Y. Gao, B. Wang, Z. Rozynek, J. O. Fossum

[17] G. Q. Yuan, H. F. Jiang, C. Lin, S. J. Liao, *J. Cryst. Growth* **2007**, *303*, 400–406.

[18] Y. Liu, Y. Chu, Y. Zhuo, M. Li, L. Li, L. Dong, *Cryst. Growth Des.* **2007**, *7*, 467–470.

[19] X. Wang, G. Xi, S. Xiong, Y. Liu, B. Xi, Y. Yu, Y. Qian, *Cryst. Growth Des.* **2007**, *7*, 930–934.

[20] X. J. Zhang, D. G. Zhang, X. M. Ni, J. M. Song, H. G. Zheng, *J. Nanopart. Res.* **2008**, *10*, 839–844.

[21] S. Jammi, S. Sakthivel, L. Rout, T. Mukherjee, S. Mandal, R. Mitra, T. Punniyamurthy, *J. Org. Chem.* **2009**, *74*, 1971–1976.

[22] P. Poizot, S. Laruelle, S. Grugeon, L. Dupont, J. M. Tarascon, *Nature* **2000**, *407*, 496–499.

[23] P. Poizot, S. Laruelle, S. Grugeon, L. Dupont, J. M. Tarascon, *J. Power Sources* **2001**, *97–98*, 235–239.

[24] J. M. Tarascon, S. Grugeon, M. Morcrette, S. Laruelle, P. Rozier, P. Poizot, *C. R. Chim.* **2005**, *8*, 9–12.

[25] A. A. Umar, M. Oyama, *Cryst. Growth Des.* **2007**, *7*, 2404–2409.

[26] Y. Chang, H. C. Zeng, *Cryst. Growth Des.* **2004**, *4*, 397–402.

[27] C. Wang, X. Q. Fu, X. Y. Xue, Y. G. Wang, T. H. Wang, *Nanotechnology* **2007**, *18*, 1455061–1455065.

[28] M. Cao, C. Hu, Y. Wang, Y. Guo, C. Guo, E. Wang, *Chem. Commun.* **2003**, 1884–1885.

[29] Y. Zhao, J. J. Zhu, J. M. Hong, N. S. Bian, H. Y. Chen, *Eur. J. Inorg. Chem.* **2004**, 4072–4080.

[30] D. Y. Han, H. Y. Yang, C. Y. Zhu, F. H. Wang, *Powder Technol.* **2008**, *185*, 286–290.

[31] Y. Chang, H. C. Zeng, *Cryst. Growth Des.* **2004**, *4*, 397–402.

[32] B. Liu, H. C. Zeng, *J. Am. Chem. Soc.* **2004**, *126*, 8124–8125.

[33] H. M. Xiao, S. Y. Fu, L. P. Zhu, Y. Q. Li, G. Yang, *Eur. J. Inorg. Chem.* **2007**, 1966–1971.